

# Quantum Monte Carlo Simulations of Fidelity at Magnetic Quantum Phase Transitions

David Schwandt,<sup>1,2</sup> Fabien Alet,<sup>1,2</sup> and Sylvain Capponi<sup>1,2</sup>

<sup>1</sup>Laboratoire de Physique Théorique, Université de Toulouse, UPS, (IRSAMC), F-31062 Toulouse, France

<sup>2</sup>CNRS, LPT (IRSAMC), F-31062 Toulouse, France

(Received 6 July 2009; revised manuscript received 14 September 2009; published 19 October 2009)

When a system undergoes a quantum phase transition, the ground-state wave function shows a change of nature, which can be monitored using the *fidelity* concept. We introduce two quantum Monte Carlo schemes that allow the computation of fidelity and its susceptibility for large interacting many-body systems. These methods are illustrated on a two-dimensional Heisenberg model, where fidelity estimators show marked behavior at two successive quantum phase transitions. We also develop a scaling theory which relates the divergence of the fidelity susceptibility to the critical exponent of the correlation length. A good agreement is found with the numerical results.

DOI: 10.1103/PhysRevLett.103.170501

PACS numbers: 03.67.-a, 02.70.Ss, 64.70.Tg, 75.10.Jm

What happens to the ground-state (GS) wave function when a physical system goes across a quantum phase transition (QPT)? Rooted in quantum information theory, the fidelity approach [1,2] provides an interesting global answer in terms of the overlap between the GS of the system at two different values of the driving parameter. The basic idea, the precursor to which may be found in Anderson's orthogonality catastrophe [3], is that quantum states become more orthogonal close to a quantum phase transition. The resulting fidelity drop can then provide a useful probe to detect the QPT. This is particularly interesting as the fidelity is a global, model-independent quantity that incorporates all the information contained in the GS wave functions. This is opposite to other usual approaches to phase transitions, which often need an input such as the knowledge of a specific order parameter.

Consider the Hamiltonian

$$H = H_0 + \lambda H_\lambda \quad (1)$$

with  $H_\lambda$  acting as a perturbation to  $H_0$ . The fidelity  $F(\lambda_1, \lambda_2)$  is defined as the modulus of the overlap between the GS of  $H$  at two different values of  $\lambda$ :

$$F(\lambda_1, \lambda_2) = |\langle \psi_0^{\lambda_1} | \psi_0^{\lambda_2} \rangle|.$$

Suppose that the system undergoes a QPT for a value  $\lambda_c$  of the driving parameter. We expect the fidelity to have a singular behavior when either  $\lambda_1$  or  $\lambda_2$  are close to  $\lambda_c$ , especially if the difference  $\delta\lambda = \lambda_2 - \lambda_1$  is small [1]. When  $\delta\lambda \rightarrow 0$ , the fidelity is dominated by its leading term, the fidelity susceptibility  $\chi_F$  [4], with  $F \approx 1 - \frac{\delta\lambda^2}{2} \chi_F$ .

When  $H$  describes a many-body system, computations of  $F$  or  $\chi_F$  are complicated. Besides a few analytical results on specific models [2], the main effort has been put into their numerical evaluation. Exact diagonalization (ED) and tensor-network (TN) methods [5]—including density matrix renormalization group (DMRG) [6]—have been the most widely used techniques in that respect, even though they suffer from several caveats. The ED method needs the full computation of the GS wave function and is therefore

limited to small systems. TN methods provide a variational ansatz for the GS wave functions, allowing a straightforward computation of overlaps. This ansatz turns out to be excellent for one-dimensional systems, where DMRG [6] in particular has proved its full strength. Recently, several TN based works studied two-dimensional ( $2d$ ) systems and their fidelity properties [7]. However, these methods remain variational and may fail in correctly capturing the GS properties of complex many-body Hamiltonians in  $d > 1$ , especially close to a QPT.

In this Letter, we present two different quantum Monte Carlo (QMC) schemes which allow an *exact* (albeit stochastic) computation of the fidelity  $F$  and its susceptibility  $\chi_F$ . We apply these methods to the antiferromagnetic (AF) Heisenberg spin model on a  $2d$  lattice. Varying one exchange coupling in the spin model causes two successive phase transitions, both of which are found to be captured by the fidelity and its susceptibility. In passing, we derive a scaling theory for the divergence of  $\chi_F$  at a second-order QPT. The two schemes benefit from the power of QMC methods, which allow us to treat very large systems *in any dimension*. The first scheme, which calculates  $F$ , is applicable to all AF systems admitting a singlet GS. The second

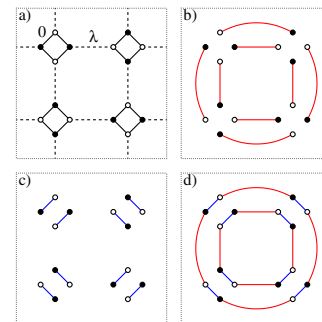


FIG. 1 (color online). (a) CaVO lattice with nearest-neighbor bonds of type  $\lambda$  (dashed lines) and 0 (solid lines). (b),(c) Typical VB states on the CaVO lattice. (d) Overlap graph of previous VB states forming two loops.

scheme for  $\chi_F$  is even more general and can be applied to several many-body problems. This opens a novel path for the fidelity approach to QPT. These techniques are only efficient when the underlying QMC method is, i.e., when there is no sign problem.

*Model.*—The schemes are illustrated on the spin-1/2 Heisenberg Hamiltonian

$$H = H_0 + \lambda H_\lambda = \sum_{\langle ij \rangle_0} \mathbf{S}_i \cdot \mathbf{S}_j + \lambda \sum_{\langle ij \rangle_\lambda} \mathbf{S}_i \cdot \mathbf{S}_j \quad (2)$$

on the CaVO lattice [8], a 1/5th depleted square lattice (see Fig. 1). The first sum runs over nearest-neighbor spins on 0 bonds (solid lines in Fig. 1) while the second is over  $\lambda$  bonds (dashed lines). This lattice structure can be found in the AF compound  $\text{CaV}_4\text{O}_9$  (hence the lattice name), even though the interactions are more complex in the real compound [9]. Varying the coupling  $\lambda$  allows the occurrence of two QPTs separating an intermediate Néel-ordered AF phase from, respectively, a low- $\lambda$  plaquette and a high- $\lambda$  dimer phase [8,10].  $H$  conserves the total spin of the system and, in particular, AF interactions  $\lambda > 0$  lead to a singlet GS.

*Fidelity measurements.*—Measuring the fidelity seems at first glance easy within a standard projection QMC scheme [11]. Decomposing the ground state  $|\psi_0^\lambda\rangle = \sum_i a_i |\varphi_i^\lambda\rangle$  in the simulation basis  $\{|\varphi\rangle\}$ , one generates representatives  $|\varphi_i^\lambda\rangle$  (i.e., in proportion of  $|a_i|$ ) of the GS via the projection scheme for two different values of  $\lambda$ . The problem comes from the fact that the QMC estimate of the fidelity  $\langle \varphi_i^{\lambda_1} | \varphi_i^{\lambda_2} \rangle$  will vanish most of the time in the commonly used orthogonal basis, leading to a serious statistical problem. However, when the GS is a singlet, it can be decomposed in the valence bond (VB) basis, which has a crucial nonorthogonality property. Indeed, any two VB states always have a nonzero fidelity  $F = |\langle \varphi_1 | \varphi_2 \rangle| = 2^{N_\ell - N/2}$  where  $N_\ell$  is the number of loops obtained by superimposing the two VB states (see Fig. 1), and  $N$  the total number of spins. This property solves the statistical problem and allows an efficient computation of the fidelity.

More specifically, we work with a VB projector loop algorithm recently proposed by Sandvik and Evertz [12]. To avoid the sign problem, we simulate nonfrustrated AF on bipartite lattices, which leads to real positive values of coefficients  $a_i \geq 0$  and of VB overlaps  $\langle \varphi_1 | \varphi_2 \rangle > 0$ . In the VB loop algorithm [12], two VB representatives  $|\varphi_L\rangle$  and  $|\varphi_R\rangle$  of the ground state are generated by propagating two initial VB states. Simulating at the same time *two* different physical systems with couplings  $\lambda_1$  and  $\lambda_2$  allows a QMC estimator of the square of the fidelity:

$$F^2(\lambda_1, \lambda_2) = \frac{\langle \varphi_L^{\lambda_1} | \varphi_R^{\lambda_2} \rangle \langle \varphi_R^{\lambda_1} | \varphi_L^{\lambda_2} \rangle}{\langle \varphi_L^{\lambda_1} | \varphi_R^{\lambda_1} \rangle \langle \varphi_L^{\lambda_2} | \varphi_R^{\lambda_2} \rangle}.$$

$F(\lambda_1, \lambda_2)$  can be computed for any value of  $\lambda_1$  and  $\lambda_2$  for all models that can be simulated with VB QMC methods.

In the following, we illustrate this method for the Heisenberg model on the CaVO lattice [Eq. (2)]. The

unit cell contains 4 spins, and we simulated square samples with  $L \times L$  unit cells (total number of spins  $N = 4L^2$ ) up to  $L = 16$ , using periodic boundary conditions. For such large systems, the fidelity essentially vanishes for all  $\lambda_1 \neq \lambda_2$ . As suggested in Ref. [13], we compute the fidelity per site  $f(\lambda_1, \lambda_2) = F(\lambda_1, \lambda_2)^{1/N}$ , which is well behaved as  $N \rightarrow \infty$ .

Our data for the fidelity per site are presented in Fig. 2. Around the diagonal where  $f(\lambda, \lambda) = 1$ , we notice the appearance of two pinch points, roughly around  $\lambda_c^1 \in [0.8, 1.1]$  and  $\lambda_c^2 \in [1.5, 1.8]$ . It has been argued that these features are characteristic of continuous QPT [13] and our results are in agreement with the two well-known second-order QPTs in this model. Far enough away from these two critical regions we notice that there is no significant change of  $f$  when  $N \rightarrow \infty$ . Within the critical regions  $f$  drops faster with system size. Given our statistical errors (up to 2% for the chosen range of  $\lambda$ ), we cannot however provide more precise ranges for the critical points. To locate more accurately the QPT, we now turn to the leading correction of fidelity around the diagonal  $\lambda_1 = \lambda_2$ .

*Fidelity susceptibility.*—For  $\delta\lambda \rightarrow 0$ , we consider the fidelity susceptibility  $\chi_F$  which can be expressed [4] as the imaginary-time integral  $\chi_F = \int_0^\infty \tau [\langle H_\lambda(0) H_\lambda(\tau) \rangle - \langle H_\lambda(0) \rangle^2] d\tau$ . This definition offers a natural extension to

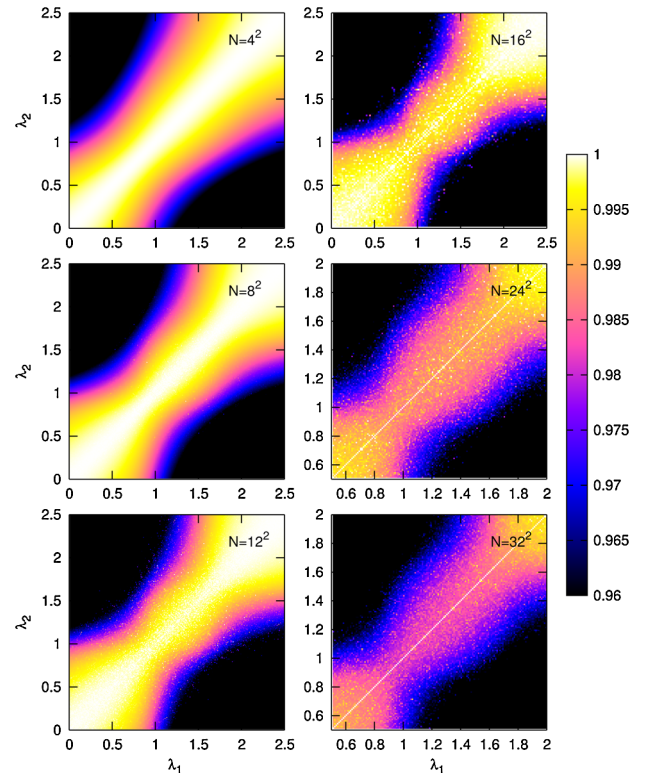


FIG. 2 (color online). Fidelity per site  $f$  as a function of  $\lambda_1$  and  $\lambda_2$  for different system sizes. Expansion power  $n$  of  $H$  in the VB QMC method is  $n/N = 20$  for  $N \leq 12^2$ ,  $10$  for  $N = 16^2$  and  $4$  for  $N \geq 24^2$ .  $\lambda$  range is  $[0, 2.5]$  for  $N \leq 16^2$  and  $[0.5, 2]$  for  $N \geq 24^2$ . Resolution  $\Delta\lambda$  for the plots is  $0.02$  for  $N = 16^2$ ,  $0.01$  otherwise.

finite temperature  $T = 1/\beta$ :

$$\chi_F(\beta) = \int_0^{\beta/2} \tau [\langle H_\lambda(0)H_\lambda(\tau) \rangle - \langle H_\lambda(0) \rangle^2] d\tau \quad (3)$$

and  $\chi_F = \lim_{\beta \rightarrow \infty} \chi_F(\beta)$ . This definition of  $\chi_F(\beta)$  differs from the Bures metric  $ds^2$  usually defined for mixed states [14], even though both have the same  $T = 0$  limit. However, one can prove [15] that  $ds^2/2 \leq \chi_F(\beta) \leq ds^2$ , showing that both quantities scale in the same way.

An advantage of Eq. (3) is that  $\chi_F(\beta)$  can be computed within a QMC stochastic series expansion (SSE) formalism [16,17]. Note the importance of taking  $\beta/2$  as the upper limit of the integral as the  $\beta$  periodicity of the path integral would lead otherwise to incorrect results. In the SSE formalism the partition function is expanded in powers of  $\beta$ ,  $Z = \sum_{n=0}^{\infty} \frac{(-\beta)^n}{n!} \text{Tr} H^n$ . Starting from the expression of time-displaced correlations functions in SSE (Eq. 3.15 of Ref. [16]),  $\chi_F(\beta)$  is estimated as

$$\chi_F(\beta) = \frac{1}{\lambda^2} \left[ \sum_{m=0}^{n-2} A(m, n) \langle N_\lambda(m) \rangle - \langle N_\lambda \rangle^2 / 8 \right], \quad (4)$$

where  $N_\lambda(m)$  is the number of times two elements of  $H_\lambda$  appear separated by  $m$  positions in the SSE sequence [16] and  $N_\lambda$  the total number of appearance of elements of  $H_\lambda$ . The amplitude  $A(m, n) = \frac{(n-1)!}{(n-m-2)!m!} \int_0^{1/2} d\tau \tau^{m+1} (1-\tau)^{n-m-2}$  can be calculated for all  $(m, n)$  prior to simulations by numerical integration or analytically for large  $n$  [15]. We emphasize that this formalism allows us to compute  $\chi_F(\beta)$  for any model which can be simulated with SSE.

The computation of  $\chi_F(\beta)$  can turn costly for large systems at low  $T$ . We reached  $L \leq 16$  and used  $\beta = 10L$

for the CaVO lattice, and limited simulations to the relevant  $\lambda$  range for the largest  $L$  and  $\beta$ .

Figures 3(a)–3(f) display the susceptibility fidelity per site  $\chi_F/N$ , showing the apparition of two peaks as a function of  $\lambda$ . While the  $N = 4^2$  and  $8^2$  samples show rather broad feature (especially for the second peak), the peaks are clearly emergent as system size is increased and temperature lowered. From the position of the two peaks for the lowest  $T$  and largest size, one obtains estimates  $\lambda_c^1 = 0.94(1)$  and  $\lambda_c^2 = 1.65(1)$  for the two quantum critical points, in full agreement with QMC computations of order parameter and spin gap [10]. Note that the positions of the maxima of  $\chi_F$  at finite  $T$  [see Figs. 3(e) and 3(f)] also allow us to determine faithfully  $\lambda_c^1$  and  $\lambda_c^2$ , even though a small shift is observed if  $\beta$  is too low. We therefore find that the fidelity susceptibility behaves as a good global indicator of QPTs in a  $2d$  quantum system.

Away from criticality,  $\chi_F$  is extensive in all phases, see Fig. 3(g). Scaling of the peaks in Fig. 3(h) reveals a power-law divergence at criticality  $\chi_F(\lambda_c)/N \sim L^\omega$ , with  $\omega = 0.73(3)$  for the first QPT and  $\omega = 0.79(6)$  for the second (error bars originate from the statistical error bar in the QMC data). This agrees with the behavior of  $f$  which develops pinch points at criticality but essentially does not change in noncritical regions as  $N \rightarrow \infty$ . The observed symmetry of the peaks around their divergence explains the hourglass shape of the pinch points in  $f$ . We also understand why the second pinch point is harder to see in Fig. 2: indeed  $\chi_F$  is much smaller close to  $\lambda_c^2$  than to  $\lambda_c^1$  (almost a factor of 2 in all cases).

*Scaling theory.*—We now account for the divergence at the QPT by formulating a finite-size scaling (FSS) theory.

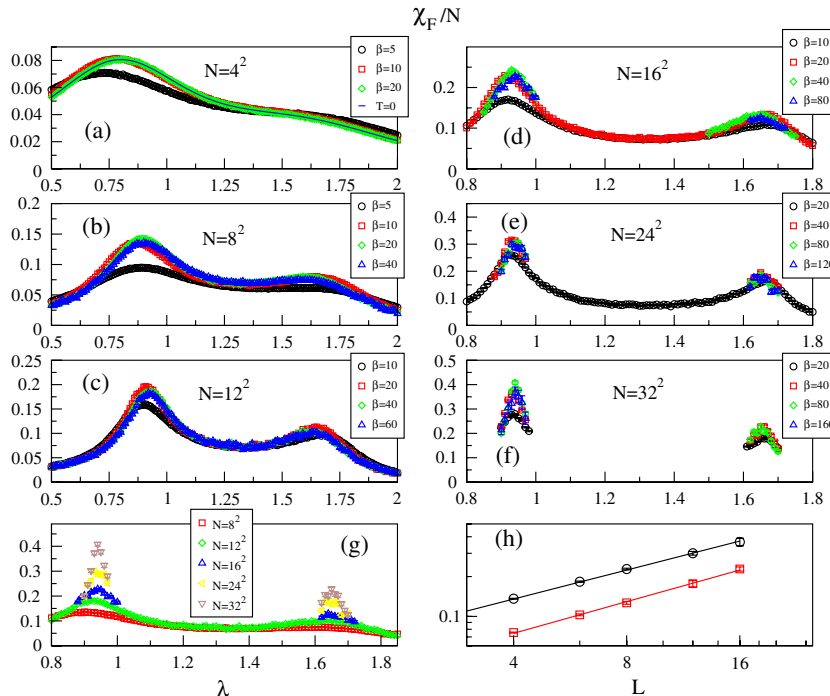


FIG. 3 (color online). (a)–(f) Fidelity susceptibility per site  $\chi_F/N$  versus  $\lambda$  for different system sizes  $N$  and inverse temperature  $\beta$ . (g)  $\chi_F/N$  versus  $\lambda$  for the largest  $\beta$  for different  $N$ . (h) Scaling of the two peaks of  $\chi_F/N$  versus linear size  $L$  (log-log scale). Lines denote power-law fits.

FSS theories for  $\chi_F$  have been proposed earlier but the relation to standard critical exponents at second-order QPT has been missed. In the most elaborate work, Campos Venuti and Zanardi [18] discuss the divergence of  $\chi_F$  as a function of the scaling dimension  $[H_\lambda]$  of the part of the Hamiltonian that drives the transition, i.e., how this operator scales at  $\lambda_c$ :  $H_\lambda \sim L^{-[H_\lambda]}$ . Here we explicitly calculate this scaling dimension. From the definition of the correlation length critical exponent  $\xi \sim (\lambda - \lambda_c)^{-\nu}$ , we have  $[\lambda] = 1/\nu$ . Noting that  $[H] = z$  where  $z$  is the dynamical critical exponent, we deduce  $[H_\lambda] = z - 1/\nu$  from Eq. (1). Finally, we conclude from Eq. (3) that  $[\chi_F] = 2[\tau] + 2[H_\lambda] = -2/\nu$  (see also Ref. [18]) and therefore  $[\chi_F/N] = -2/\nu + d$ , leading to the prediction:

$$\chi_F(\lambda_c)/N \sim L^{2/\nu-d}. \quad (5)$$

This relation should hold for all second-order QPTs and explains the superextensive behavior generally observed for  $\chi_F$  in terms of the usual critical exponents. From the value  $\nu \simeq 0.7112$  of the universality class of the  $3d$   $O(3)$  model [19] to which belong both QPTs studied here, we expect from this analysis  $\omega \simeq 0.812$ , in agreement with our numerical estimates.

*Discussions and conclusion.*—In conclusion, we presented two QMC schemes that are able to calculate with high accuracy the fidelity and its susceptibility for quantum interacting systems, in any dimension. This allows us to pin down the behavior of fidelity at QPT, using one of the most sophisticated numerical techniques for the many-body problem. Taking the example of the Heisenberg model on the CaVO lattice, we find that both  $F$  and  $\chi_F$  are able to locate the two quantum critical points present in this system. The fidelity susceptibility acts as a more precise indicator as criticality manifests itself as a marked peak in  $\chi_F$ . However, there is in principle more information contained in  $F$ . This could be useful to detect transitions that  $\chi_F$  does not capture [20], as well as in the context of quantum quenches [21,22].

The divergence of  $\chi_F$  at criticality is accounted for by the scaling theory that we have presented, where the connection to the correlation length exponent of the universality class of the QPT is made. We also showed that the generalization of  $\chi_F$  to finite temperature [Eq. (3)] allows us to detect criticality for moderate values of  $T$ . This is of practical interest as simulations can be performed at a smaller computational cost.

The method proposed for measuring  $\chi_F$  works for any model which can be simulated within the generic SSE scheme [16,17], opening the door to the study of fidelity in many different physical systems. We expect that our scheme can be extended to measure the Loschmidt echo, another witness of quantum criticality [23], which can be measured experimentally in this context [24].

We thank F. Albuquerque, A. Läuchli, O. Motrunich, G. Roux and C. Sire for very useful discussions. Calculations were performed using the ALPS libraries [25]. We

thank GENCI and CALMIP for allocation of CPU time. This work is supported by the French ANR Program No. ANR-08-JCJC-0056-01.

*Note added.*—The scaling relation Eq. (5) has been independently derived in recent preprints [22].

- 
- [1] P. Zanardi and N. Paunković, Phys. Rev. E **74**, 031123 (2006); P. Zanardi, P. Giorda, and M. Cozzini, Phys. Rev. Lett. **99**, 100603 (2007).
  - [2] For a review, see S.-J. Gu, arXiv:0811.3127.
  - [3] P. W. Anderson, Phys. Rev. Lett. **18**, 1049 (1967).
  - [4] W.-L. You, Y.-W. Li, and S.-J. Gu, Phys. Rev. E **76**, 022101 (2007).
  - [5] For a review, see F. Verstraete, V. Murg, and J.I. Cirac, Adv. Phys. **57**, 143 (2008); Recent advances include J. Jordan *et al.*, Phys. Rev. Lett. **101**, 250602 (2008); H.-C. Jiang, Z.-Y. Weng, and T. Xiang, *ibid.* **101**, 090603 (2008); R. Orús, A.C. Doherty, and G. Vidal, *ibid.* **102**, 077203 (2009); Z.-C. Gu, M. Levin, and X.-G. Wen, Phys. Rev. B **78**, 205116 (2008).
  - [6] S. R. White, Phys. Rev. Lett. **69**, 2863 (1992).
  - [7] H.-Q. Zhou, R. Orús, and G. Vidal, Phys. Rev. Lett. **100**, 080601 (2008); B. Li, S.-H. Li, and H.-Q. Zhou, Phys. Rev. E **79**, 060101(R) (2009); J. Jordan, R. Orús, and G. Vidal, Phys. Rev. B **79**, 174515 (2009).
  - [8] K. Ueda *et al.*, Phys. Rev. Lett. **76**, 1932 (1996).
  - [9] K. Kodama, J. Phys. Soc. Jpn. **66**, 793 (1997); M. A. Korotkin *et al.*, Phys. Rev. Lett. **83**, 1387 (1999).
  - [10] M. Troyer, H. Kontani, and K. Ueda, Phys. Rev. Lett. **76**, 3822 (1996); M. Troyer, M. Imada, and K. Ueda, J. Phys. Soc. Jpn. **66**, 2957 (1997).
  - [11] N. Trivedi and D.M. Ceperley, Phys. Rev. B **40**, 2737 (1989).
  - [12] A. W. Sandvik and H. G. Evertz, arXiv:0807.0682.
  - [13] H.-Q. Zhou and J.-P. Barjaktarevic, J. Phys. A **41**, 412001 (2008); H.-Q. Zhou, J.-H. Zhao, and B. Li, *ibid.* **41**, 492002 (2008).
  - [14] P. Zanardi, L. Campos Venuti, and P. Giorda, Phys. Rev. A **76**, 062318 (2007).
  - [15] F. Albuquerque *et al.* (to be published).
  - [16] A. W. Sandvik, J. Phys. A **25**, 3667 (1992).
  - [17] A. W. Sandvik, Phys. Rev. B **59**, R14157 (1999).
  - [18] L. Campos Venuti and P. Zanardi, Phys. Rev. Lett. **99**, 095701 (2007).
  - [19] M. Campostrini *et al.*, Phys. Rev. B **65**, 144520 (2002).
  - [20] Y.-C. Tzeng *et al.*, Phys. Rev. A **77**, 062321 (2008).
  - [21] A. Peres, Phys. Rev. A **30**, 1610 (1984); G. Roux, arXiv:0909.4620.
  - [22] C. De Grandi, V. Gritsev, and A. Polkovnikov, arXiv:0909.5181, arXiv:0910.0876; R. Barankov, arXiv:0910.0255.
  - [23] H. T. Quan *et al.*, Phys. Rev. Lett. **96**, 140604 (2006).
  - [24] J. Zhang *et al.*, Phys. Rev. A **79**, 012305 (2009).
  - [25] F. Albuquerque *et al.*, J. Magn. Magn. Mater. **310**, 1187 (2007); M. Troyer, B. Ammon, and E. Heeb, Lect. Notes Comput. Sci. **1505**, 191 (1998); F. Alet, S. Wessel, and M. Troyer, Phys. Rev. E **71**, 036706 (2005); see <http://alps.comp-phys.org>.